Graphical Design Applied to MTBE and Methyl Acetate Reactive Distillation Processes

Jae W. Lee and Arthur W. Westerberg
Dept. of Chemical Engineering and Institute for Complex Engineered Systems, Carnegie Mellon University, Pittsburgh, PA 15213

Graphical tray-by-tray methods for reactive distillation columns we developed previously are extended to study two industrial processes: MTBE production and methyl acetate production. As both processes involve four components, projection was used to obtain ternary diagrams by ignoring the inert (n-butane) for MTBE production and by projecting onto planes of constant acetic acid concentrations for methyl acetate production. These projected methods clearly explain the placing that industry uses for the reaction zones in these processes. Further, it can be visualized why there is an optimum reflux ratio for the methyl acetate process and a value can be quantitatively predicted for it that lies within the range the literature reports.

Introduction

In earlier studies we have noted the interest in reactive distillation that arose when the Eastman Chemical Company won the Kirkpatrick award for their new design of the methyl acetate process (Agreda and Partin, 1984; Agreda et al., 1990). In our own work, we have developed graphical methods to study reactive distillation. Lee et al. (2000a) derived a reactive lever rule from the linear combinations of composition vectors. McCabe-Thiele and Pochon-Savarit methods were adapted for reactive distillation (Lee et al., 2000b, c). These binary diagrams illustrated how a synergistic effect of reaction and separation eliminates an azeotrope (Lee et al., 2000d). Some design insights for binary reactive distillation columns are as follows: (1) With the isomerization reaction with a heavy reactant, the reaction zone in the rectifying section made separation easier (Lee et al., 2000e); (2) Binary azeotropes can be circumvented under a finite reflux (but not under total reflux) and with a reasonable range of reaction equilibrium constants (Lee et al., 2000f). However, for practical applications, these graphical methods should be extended into ternary or quaternary reactive systems. Recently, Lee and Westerberg (2000g) proposed tray-by-tray calculations for ternary isomolar reacting mixtures by assuming constant molar overflow. They introduced the reaction equilibrium curve and the corresponding V/L equilibrated bubble point curve to confine vapor and liquid compositions of each reactive stage to these two curves. In this article we shall extend our graphical method into quaternary reactive systems and apply it to study two four-component systems: MTBE and methyl acetate production systems.

Our studies will be in composition space. For four components, this space is a tetrahedron, a three-dimensional (3-D) construct. Graphical methods in a 3-D space, while possible, are not comfortable for most people. Therefore, we stress in this article how we can reduce the diagrams to allow the study of triangular diagrams.

We shall first study the MTBE process. It is a nonisomolar process that involves three reactive species and one inert. To study this process graphically, we shall ignore the inert species. The methyl acetate is an equimolar reaction involving four species. We shall analyze the behavior of this process and discover that we can strategically project composition space onto a plane of low acetic acid concentration. On that projection, we shall show why there is a best value for the reflux ratio in this column. We will be able to argue why the projected information allows us to derive the needed insights even though the tray-by-tray calculations are not isolated within that plane. We shall quantitatively find a value for that reflux ratio that places it in the range discussed in the Eastman report (Agreda et al., 1990). We shall use computer simulations of the actual reacting systems to confirm our graphical insights.

MTBE, a Nonisomolar Equilibrium Reaction

Methyl *tert*-butyl ether (MTBE) can be produced from iso-butene (IBUT) and methanol (MeOH) under an acid cat-

Correspondence concerning this article should be addressed to A. W. Westerberg.

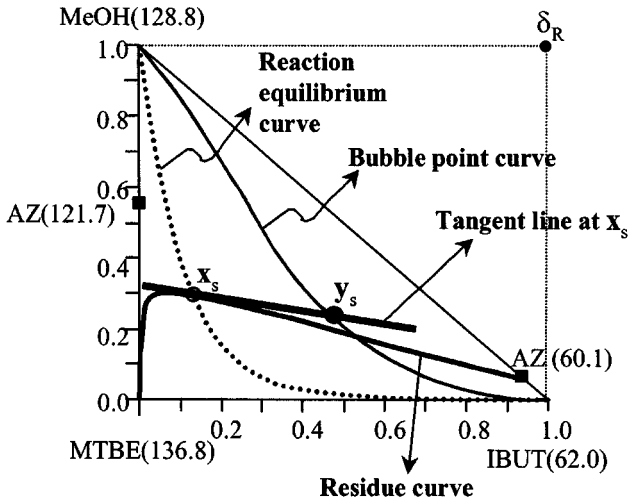

Figure 1. Reaction equilibrium and its corresponding bubble point curve for MTBE production system at 8 atm.

( ): Boiling points in celsius degree.

alyst (Al-Jarallah et al., 1988) or an ion-exchange resin (Rehfinger and Hoffmann, 1990) as in Eq. 1.

$$\mathrm{MeOH}(CH_3OH) + \mathrm{IBUT}(i-C_4H_8) \Leftrightarrow \mathrm{MTBE}(C_5H_{12}O) \tag{1}$$

This reaction occurs in the liquid phase. Equation 2 gives the reaction equilibrium constant as a function of temperature (Venimadhavan et al., 1994).

$$\ln(K_{eq}) = \frac{6{,}820.0}{T} - 16.33, \ (T = \text{Kelvin}) \tag{2}$$

There are two minimum boiling azeotropes, MeOH-MTBE (55.8 mol % of MeOH) and MeOH-IBUT (93.2 mol % of IBUT) at 8 atm, as estimated by the Wilson property set in Aspen Plus.

Figure 1 shows the reaction equilibrium curve, which corresponds to all liquid compositions that are simultaneously in chemical equilibrium and at their bubble points. Points on the bubble point curve are the vapor compositions in phase equilibrium with these liquid compositions. The tangent line to the residue curve passing through a liquid composition such as x_s intersects the bubble point curve at y_s, the vapor in phase equilibrium with x_s.

The procedure for tray-by-tray calculations for this nonisomolar reaction is similar to that in our previous study for an isomolar reaction (Lee and Westerberg, 2000g), except here the reaction difference point ($\delta_R = \boldsymbol{\nu}/\upsilon_T = [-1,-1,1]^T/-1 = [1,1,-1]^T$) is finite. As noted in our earlier articles, this difference point has a physical interpretation; it is the composition for a pseudo-stream whose flow corresponds to the reactants leaving the column and the products entering in stoichiometric amounts. It lies outside the feasible composition space, as it has negative and positive compositions in it. The flow ξ for such a stream is the reaction turnover (or reaction extent).

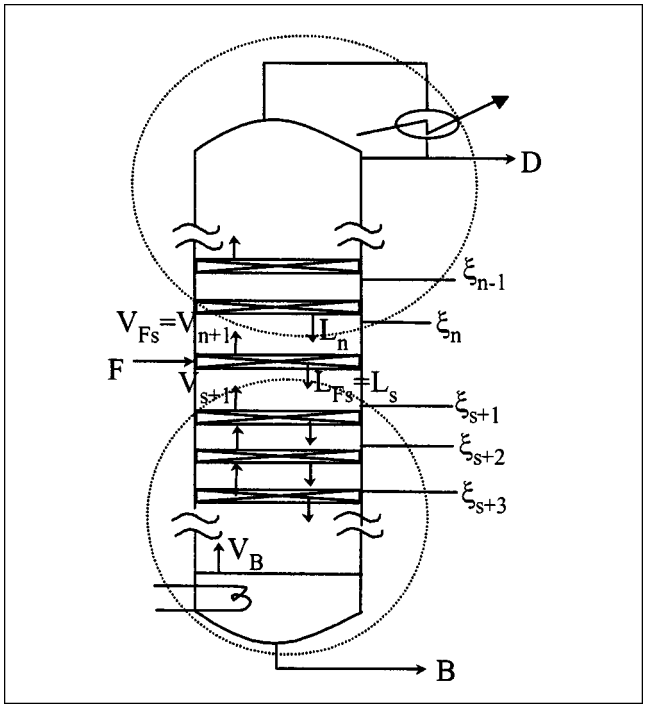

Figure 2. Reactive distillation column.

We use material balances around the rectifying in Figure 2 to write the following equations

$$V_{n+1}y_{n+1} = x_n L_n + (D - \nu_T \xi_n)\delta^r_{R,n} \tag{3}$$

which defines the cascade difference point ($\delta^r_{R,n}$, a "composition") as

$$(D - \nu_T \xi_n)\delta^r_{R,n} = Dx_D - V_T \xi_n \delta_R \tag{4}$$

and similarly for the stripping section

$$L_s x_s = V_{s+1} y_{s+1} + (B - \nu_T \xi_{s+1})\delta^s_{R,s+1} \tag{5}$$

$$(B - \nu_T \xi_{s+1})\delta^s_{R,s+1} = Bx_B - \nu_T \xi_{s+1}\delta_R \tag{6}$$

Our goal is to produce relatively pure products so we need to design our columns so that the total "flow" of the forward reaction is larger than the total "flow" of the backward reaction. Thus, the reaction extent (ξ) will ultimately increase as we include more and more trays in a balance. If we place reactive trays in the top of the column, $\delta^r_{R,n}$ should ultimately move toward the reaction difference point (δ_R) as we go down the column from the top stage. Similarly, if we place reactive trays in the bottom of the column, $\delta^s_{R,s+1}$ should move toward the reaction difference point as we move up the column from the bottom stage.

Reaction distribution to circumvent azeotropes in the methyl tert-butyl ether production system

In the MTBE production system, the heat of reaction, as well as reaction itself, affects the liquid and vapor flow rates on reactive stages. Thus, internal reflux ratios vary on each

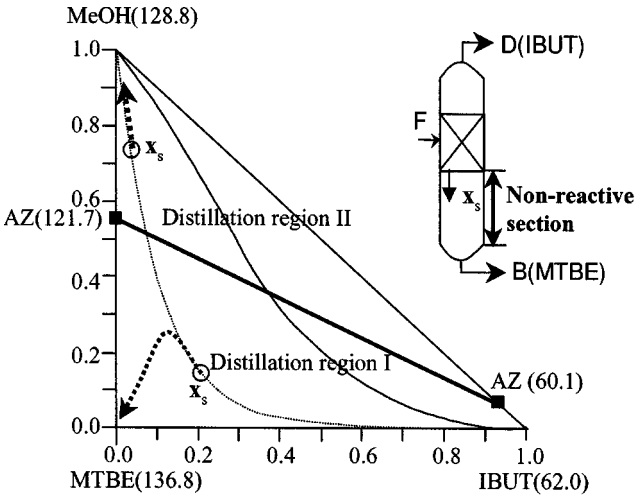

Figure 3. Two possible liquid trajectories from reactive to nonreactive sections.

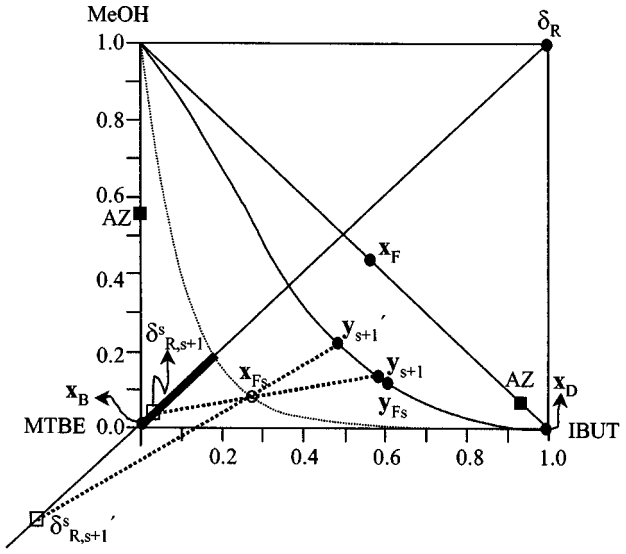

Figure 4. Reverse reaction can occur in the stripping section.

As the reboil ratio increases, the reverse reaction becomes dominant.

reactive stage, and we should include the heat balance in our tray-by-tray calculations. However, if we scrutinize the positions of the reaction equilibrium curve, its corresponding bubble point curve, and the trajectory of reactive cascade difference points, we can obtain design insights into where we should place reaction zones with simple sketches.

The goal of reaction distribution is to produce pure IBUT and MTBE at the top and bottom, respectively, of a single-feed reactive distillation column. Start at some liquid composition on the reactive equilibrium curve. We label such a point x_s in Figure 3. Assume it is at the lowest reactive stage of the column. If it resides in distillation region I, then a nonreactive section in the stripping section will make it possible to produce pure MTBE at the bottom of the column, where MTBE is the highest boiling node in region I. However, if the liquid composition x_s lies within distillation region II, the bottom product will be MeOH because it represents the highest boiling node in distillation region II. Thus, it is relatively easy to produce pure MTBE at the bottom: (1) if the final liquid composition at the lowest reactive stage lies within distillation region I; and (2), if for the needed further purification of the reactive liquid mixture to obtain pure MTBE, we include a nonreactive section below the reaction zone. If we look at diagrams for constant amounts of n-butane diluting these mixtures, the structure of the triangular diagram does not change and allows us to draw the same conclusions.

We need to ask next how to produce pure excess IBUT at the top. We could accomplish this if we can find trajectories that will bring the top of the column to right side of the lower edge of the composition diagram. Can we accomplish this goal by the proper distribution of the reactive section?

We shall start by examining in more detail placing reaction in the stripping section. We consider the geometric implications of Eqs. 5 and 6, looking first at Eq. 6. We wish for our column to produce product (MTBE) so we want a net overall forward reaction in the column—that is, we want ξ characterizing the reaction turnover to be positive when we consider the whole column. For the particular case of reaction in the bottom of the column, we should first assess where the reaction turnover (ξ_{s+1}) in Eq. 6 is positive. See Figure 4. Equation 6 states that the reaction difference point (δ_R), the bottoms product composition (x_B), and any reactive cascade difference point ($\delta^s_{R,s+1}$) must all lie on the same straight line. By examining the signs (remember v_T is negative), one can note that the reaction turnover is positive when the reactive cascade difference point (that is, the composition of the reaction turnover) lies between the reaction difference point (δ_R) and the bottom product composition (x_B). Equation 5 further implies that, if the reaction turnover is positive, then the liquid composition (x_s) must lie between the vapor composition (y_{s+1}) and the reactive cascade difference point ($\delta^s_{R,s+1}$). Thus, the reactive cascade difference point has to lie to the left of the liquid reaction equilibrium curve. We discover that, for a positive reaction turnover, the location for a feasible reactive cascade difference point is very limited —to between the bottom product composition x_B and liquid reaction equilibrium curve. The bold portion of the line joining δ_R and x_B is this range.

Look again at the line along which the reactive cascade difference point must lie. Equation 6 says that the length of the line segment between x_B and $\delta^s_{R,s+1}$ is related to the amount of reaction turnover (ξ_{s+1}), while the length of the segment between $\delta^s_{R,s+1}$ and δ_R is the relative bottom product flow rate. The line segment corresponding to the reaction turnover has to be short relative to the other segment; thus, there can be very little net positive reaction possible in the bottom of the column.

Assume the feed stage is reactive. Therefore, its liquid composition lies on the reaction equilibrium curve. We pick (arbitrarily) such a point on Figure 4 and label it x_{Fs}. For a given reboil ratio (which establishes the relative length of the line segments), the corresponding vapor composition is y_{s+1}. For this placement, we note that the cascade different point

for a positive turnover lies very close to x_B. Furthermore, as the reboil ratio increases, the location of the reactive cascade difference point ($\delta^{s}_{R,s+1}{}'$) can move past the bottom product composition to the left and down. In this case, ξ_{s+1} has a negative value, and the reverse reaction dominates. If we elect to have a dominating reverse reaction here, we will have to counter its effects elsewhere in the column to have the column produce MTBE. Thus, the stripping reaction zone can result in a small conversion, as well as the reverse reaction.

We shall observe now that we can obtain pure IBUT if the reaction zones are in the feed and rectifying sections since the reaction on each reactive stage in the rectifying section forces the liquid compositions on the reaction equilibrium curve to stay near the binary edge of MTBE-IBUT in Figure 5. To make our arguments, we examine the implications of 3 and 4. Equation 4 says the reactive cascade difference point ($\delta^{r}_{R,n}$), the top product composition (x_D), and the reaction difference point (δ_R) are on a straight line—here, vertically, along the right edge. Equation 3 says that the reactive cascade difference point ($\delta^{r}_{R,n}$) and the opposing liquid and vapor compositions (x_n and y_{n+1} or y_{Fs}) between trays in the rectifying section are on another straight line. Equation 4 further says that, for a net forward reaction, the reactive cascade difference point will always be between x_D and δ_R. In Figure 5 we can see then that, for a reactive tray, the vapor composition (y_{Fs}) is then always between the liquid composition (x_n) and the reactive cascade difference point ($\delta^{r}_{R,n}$), which is consistent with Eq. 3. The line connecting $\delta^{r}_{R,n}$ and x_D (representing ξ_n) is longer than the line connecting $\delta^{r}_{R,n}$ and δ_R (representing D). Thus, the reaction turnover (ξ_n) is larger than D and the forward reaction occurs more dominantly in the rectifying section than in the stripping section. Furthermore, if there is no reaction in the rectifying section, the vapor composition of the feed stage lies between the straight line connecting the distillate composition and the liquid composition (x^*_n), and the equilibrated vapor composition (y^*_n) will move close to the azeotropic composition. Hence, it is difficult to circumvent this azeotrope as shown in Figure 5, if there is no reaction in the rectifying section.

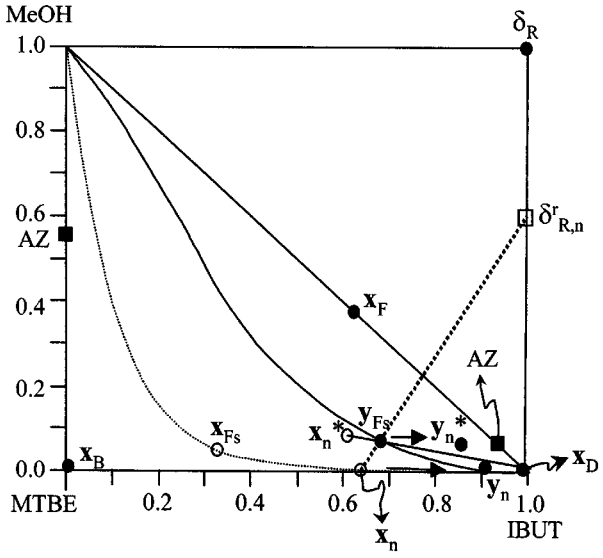

Figure 5. Circumventing the binary azeotrope of IBUT-MeOH by placing the reaction in the rectifying section.

x^*_n and y^*_n are the liquid and vapor compositions at stage n if there is no reactive stage in the rectifying section.

In summary, to produce pure IBUT at the top and pure MTBE at the bottom, the reaction zones should be in the feed and rectifying sections. This is why industry uses an ion-exchange catalyst rather than an acid liquid catalyst (Smith, 1981, 1992; Nocca et al., 1989; Preston, 1998). If we inject the acid liquid catalyst into the top section, the reaction will oc-

Table 1. Simulation Results for MTBE Production System Under Reaction Equilibrium

Reaction Zones	Feed & Rectifying	Feed & Stripping	Feed & Stripping
Feed flow rate (kmol/h) IBUT/MeOH	1,200/1,000	1,200/1,000	1,200/1,000
Product:			
Top flow/IBUT purity	200/99.8	200/93.7	200/93.7
Btm flow/MTBE purity	1,003.4/99.2	1,014.5/97.1	1,046.3/91.1
Total stage No.	14	14	14
Feed stage	4	4	4
Reactive stages	2–4	4–6	4–12
Reflux ratio	18	18	18
Duty (GJ/h):			
Condenser	67.10	70.73	70.73
Reboiler	35.54	38.69	38.30
Reactive stage no./net reaction turnover, $\Delta\xi_n$ (kmol/h)	2/4.31 3/64.32 4/927.96	4/985.38 5/0.11 6/−0.03	4/985.43, 5/0.17 6/0.40, 7/0.94 8/2.22, 9/5.34 10/12.23, 11/22.32 12/-75.35
Total molar reaction conversion based on MeOH feed	99.7%	98.5%	93.1%

cur from that injected section to the bottom since this acid liquid catalyst goes down from the injection point.

Table 1 shows simulation results for three cases with different locations of reaction zones. The reflux ratio, the total number of stages, and the location of the feed stage remain unchanged in each case. The reaction zone in the feed and rectifying sections leads us to produce nearly pure IBUT and MTBE. The second column in Table 1 has the same number of reactive stages as the first column, but it has reaction zones in the feed and stripping sections. The distillate composition (93.7% of IBUT) is close to the azeotropic composition (93.2% of IBUT-6.8% of MeOH), which means if more nonreactive stages are added at the top, the top product composition approaches the azeotrope. Thus, it is hard for the feed and stripping reactive sections to eliminate the binary azeotrope between IBUT and MeOH. As already explained in Figure 4, the net reaction turnover in the stripping section is very small as shown in the second column of Table 1 (at stages 5 and 6, nearly zero). If the number of stripping reactive stages increases as in the third column of Table 1, the total reaction conversion and product purities will decrease due to the dominant reverse reaction of the final reactive stage ($\Delta\xi_{12}$ in the third column of Table 1 is -75.35 kmol/h).

Visualization of a High-Dimensional Composition Space

In this section, we shall derive and generalize a projection method to visualize a high-dimensional composition space for multiple reactions.

Modified phase equilibrium in the projected space

The projected space is cut from the original composition space by fixing one or more of the liquid compositions of nonkey components. In the original composition space, the equilibrated vapor compositions with the liquid compositions on the projected space do not lie on the projected space except azeotropic compositions. Figure 6 shows the projection of a vapor composition into a triangle in a quaternary mixture. To project this vapor composition into the reduced space, we need to modify the V/L equilibrium relationship.

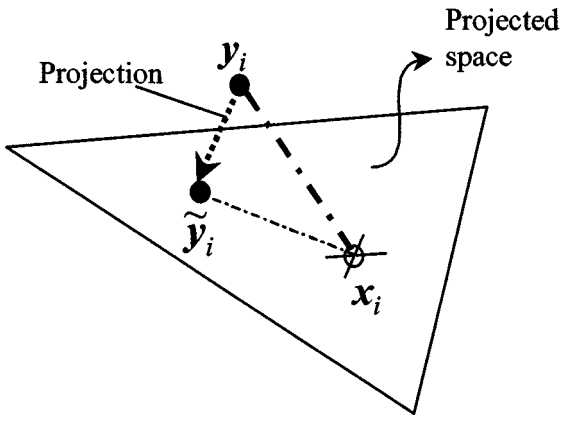

Figure 6. Projection of the equilibrated vapor compositions into the projected space.

In the original composition space, the phase equilibrium is given by

$$y_i = K_i x_i,\ i = 1\ldots,\ c \tag{7}$$

In the projected space with the constant liquid compositions of nonkey components (x_k), the liquid composition and vapor composition are as follows

$$\tilde{x}_l = x_i \Big/ \left(1 - \sum_k^{c-m} x_k\right) \tag{8}$$

$$\tilde{y}_l = y_i \Big/ \left(1 - \sum_k^{c-m} y_k\right) = y_i \Big/ \left(1 - \sum_k^{c-m} K_k x_k\right) \tag{9}$$

The value for m will generally be three as we can most readily visualize the triangular composition space for three components. If we substitute Eqs. 8 and 9 into Eq. 7 we can obtain Eqs. 10 and 11 for the projected space

$$\tilde{y}_l = K'_l \tilde{x}_l,\ l = 1\ldots,\ m \tag{10}$$

where

$$K'_l = K_l \left(1 - \sum_k^{c-m} x_k\right) \Bigg/ \left(1 - \sum_k^{c-m} K_k x_k\right) \tag{11}$$

Thus, the equation of the residue curve map in the projected space becomes

$$\frac{d\tilde{x}_l}{d\theta} = \tilde{x}_l - K'_l \tilde{x}_l,\ l = 1\ldots,\ m \tag{12}$$

Projection equations from balance equations

Here, we derive the equations for tray-by-tray calculations of a reactive section and the total balance around a whole column in a projected subspace. The following multiple reactions are assumed to occur in a double-feed reactive distillation column.

$$\sum_{i=1}^{Nr} a_{ij} R_i \Leftrightarrow \sum_{k=1}^{Np} b_{kj} P_k, j = 1,2,\ \ldots,\ NR \tag{13}$$

We need to distinguish between reactions for which there is no net change of moles (having a sum of stoichiometric coefficients υ_T equal to zero) and those for which there is, as the reaction difference point is at infinity for the former. The balance equations around the reaction zone between two feedstreams (E and F) are as follows

$$V_{n+1} = L_n + D - E - V_T^T \Xi_n \tag{14}$$

$$V_{n+1} y_{n+1} = L_n x_n + D x_D - E x_E - V \Xi_n \tag{15}$$

V_T is a column vector whose elements are the sum of the stoichiometric coefficients for the NR reactions. V is a matrix whose columns are the stoichiometric coefficient vectors for the NR reaction. Ξ_n is a column vector whose elements are the accumulated reaction turnovers for the reactions. Here, y_{n+1} is the vapor composition vector at stage $n+1$. If we decompose the term $V\Xi_n$ in Eq. 15 by considering the nonzero and zero values of the elements in vector V_T, we can obtain Eq. 16, using the lever rule equations derived by Lee et al. (2000a). For clarification, the number of reactions (NR) is the sum of Z and NZ, where Z is the number of reactions having no net change in moles, resulting in a zero element in V_T, and NZ is the number of reactions with nonzero elements in V_T. b_{kj} is the stoichiometric coefficient for product k and reaction j. a_{ij} is the stoichiometric coefficient for reactant i and reaction j

$$V\Xi_n = \left(V_{TNZ}^T \Xi_{nNZ} \delta_{RMn} + \sum_{j=1}^{Z} \left(\xi_{nj} \sum_{i=1}^{Nr} a_{ij} \right) (c_{PMn} - c_{RMn}) \right) \tag{16}$$

where

$$\Xi_{nNZ} = [\, \xi_{n1}, \ldots, \xi_{nNZ} \,]^T \tag{17}$$

$$\delta_{RMn} = \left(\sum_{j=1}^{NZ} \left(\xi_{nj} \delta_{Rj} \left(\sum_{k=1}^{Np} b_{kj} - \sum_{i=1}^{Nr} a_{ij} \right) \right) \right) \Big/ \left[V_{TNZ}^T \Xi_{nNZ} \right] \tag{18}$$

$$c_{PMn} = \sum_{j=1}^{Z} \left(\sum_{i=1}^{Nr} a_{ij} \xi_{nj} c_{Pj} \right) \Big/ \left(\sum_{j=1}^{Z} \sum_{i=1}^{Nr} a_{ij} \xi_{nj} \right) \tag{19}$$

$$c_{RMn} = \sum_{j=1}^{Z} \left(\sum_{i=1}^{Nr} a_{ij} \xi_{nj} c_{Rj} \right) \Big/ \left(\sum_{j=1}^{Z} \sum_{i=1}^{Nr} a_{ij} \xi_{nj} \right) \tag{20}$$

Using the normalized key components, $\tilde{x}_n$, $\tilde{y}_{n+1}$, $\tilde{\delta}_{RMn}$, $\tilde{c}_{PMn}$ and $\tilde{c}_{RMn}$ which are $x_n/(1-\Sigma x_{n,k})$, $y_{n+1}/(1-\Sigma y_{n+1,k})$, $\delta_{RMn}/(\Sigma \delta_{RMn,k})$, $c_{PMn}/(1-\Sigma c_{PMn,k})$ and $c_{RMn}/(1-\Sigma c_{RMn,k})$, we can rewrite Eq. 15 as follows

$$\begin{aligned} V_{n+1} \left(1 - \sum_{k}^{c-m} y_{n+1,k} \right) \tilde{y}_{n+1} &= L_n \left(1 - \sum_{k}^{c-m} x_{n,k} \right) \tilde{x}_n \\ &+ D \left(1 - \sum_{k}^{c-m} x_{D,k} \right) \tilde{x}_D - E \left(1 - \sum_{k}^{c-m} x_{E,k} \right) \tilde{x}_E \\ &- V_{TNZ}^T \Xi_{nNZ} \left(1 - \sum_{k}^{c-m} \delta_{RMn,k} \right) \tilde{\delta}_{RMn} \\ &- \sum_{j=1}^{Z} \xi_{nj} \sum_{i=1}^{Nr} a_{ij} \left(\left(1 - \sum_{k}^{c-m} c_{PMn,k} \right) \tilde{c}_{PMn} \right. \\ &\left. - \left(1 - \sum_{k}^{c-m} c_{RMn,k} \right) \tilde{c}_{RMn} \right) \end{aligned} \tag{21}$$

Equation 21 can be simplified into Eq. 22 by introducing new variables

$$\tilde{V}_{n+1} \tilde{y}_{n+1} = \tilde{L}_n \tilde{x}_n + \tilde{D} \tilde{x}_D - \tilde{E} \tilde{x}_E - \tilde{R}_n \tilde{\delta}_{TMn} \tag{22}$$

$$\tilde{V}_{n+1} = V_{n+1} \left(1 - \sum_{k}^{c-m} y_{n+1,k} \right) \tag{23}$$

$$\tilde{L}_n = L_n \left(1 - \sum_{k}^{c-m} x_{n,k} \right) \tag{24}$$

$$\tilde{D} = D \left(1 - \sum_{k}^{c-m} x_{D,k} \right) \tag{25}$$

$$\tilde{E} = E \left(1 - \sum_{k}^{c-m} x_{E,k} \right) \tag{26}$$

$$\begin{aligned} \tilde{R}_n &= V_{TNZ}^T \Xi_{nNZ} \left(1 - \sum_{k}^{c-m} \delta_{RMn,k} \right) \\ &+ \sum_{j}^{Z} \xi_{nj} \sum_{i=1}^{Nr} a_{ij} \left(\sum_{k}^{c-m} c_{RMn,k} - \sum_{k}^{c-m} c_{PMn,k} \right) \end{aligned} \tag{27}$$

$$\tilde{\delta}_{TMn} = \frac{V_{TNZ}^T \Xi_{nNZ} \left(1 - \sum_{k}^{c-m} \delta_{RMn,k} \right) \tilde{\delta}_{RMn} + \left(\sum_{j}^{Z} \xi_{nj} \sum_{j}^{Nr} a_{ij} \left(\left(1 - \sum_{k}^{c-m} c_{PMn,k} \right) \tilde{c}_{PMn} - \left(1 - \sum_{k}^{c-m} c_{RMn,k} \right) \tilde{c}_{RMn} \right) \right)}{V_{TNZ}^T \Xi_{nNZ} \left(1 - \sum_{k}^{c-m} \delta_{RMn,k} \right) + \sum_{j}^{Z} \xi_{nj} \sum_{i=1}^{Nr} a_{ij} \left(\sum_{k}^{c-m} c_{RMn,k} - \sum_{k}^{c-m} c_{PMn,k} \right)} \tag{28}$$

Here, $\tilde{V}_{n+1}$, $\tilde{L}_n$, $\tilde{D}$, $\tilde{E}$ and $\tilde{R}_n$ are the vapor, the liquid, the distillate, the upper feed and the reaction-generated flow rates in a projected space. $\tilde{\delta}_{TMn}$ is the total cascade difference point at stage n in this subspace. The subscript k in all terms means excluded components in the projected space.

We can easily derive the total balance equations for projected spaces in the same way as we derive the stagewise balance equations. From starting Eqs. 29 and 30 for the original composition space (Lee et al., 2000a), we obtain the following final balance equations

$$F_t = E + F = D + B - V_T^T \Xi \tag{29}$$

$$\begin{aligned} F_t x_{Ft} &= D x_D + B x_B - \left(V_{TNZ}^T \Xi_{NZ} \delta_{RM} \right. \\ &\left. + \sum_{j=1}^{Z} \left(\xi_j \sum_{i=1}^{Nr} a_{ij} \right) (c_{PM} - c_{RM}) \right) \end{aligned} \tag{30}$$

$$\tilde{F}_t \tilde{x}_{Ft} = \tilde{D}\tilde{x}_D + \tilde{B}\tilde{x}_B - \tilde{R}\tilde{\delta}_{TM} \tag{31}$$

where

$$\tilde{F}_t = F_t\left(1 - \sum_k^{c-m} x_{Ft,k}\right) \tag{32}$$

$$\tilde{B} = B\left(1 - \sum_k^{c-m} x_{B,k}\right) \tag{33}$$

$$\tilde{R} = V_{TNZ}^T \Xi_{NZ}\left(1 - \sum_k^{c-m} \delta_{RM,k}\right) + \sum_j^{Z} \xi_j \sum_{k=1}^{Nr} a_{ij}\left(\sum_k^{c-m} c_{RM,k} - \sum_k^{c-m} c_{PM,k}\right) \tag{34}$$

where

$$\tilde{\delta}_{TM} = \frac{V_{TNZ}^T \Xi_{NZ}\left(1 - \sum_k^{c-m} \delta_{RM,k}\right)\tilde{\delta}_{RM} + \left(\sum_j^{Z} \xi_j \sum_i^{Nr} a_{ij}\left(\left(1 - \sum_k^{c-m} c_{PM,k}\right)\tilde{c}_{PM} - \left(1 - \sum_k^{c-m} c_{RM,k}\right)\tilde{c}_{RM}\right)\right)}{V_{TNZ}^T \Xi_{NZ}\left(1 - \sum_k^{c-m} \delta_{RM,k}\right) + \sum_j^{Z} \xi_j \sum_{i=1}^{Nr} a_{ij}\left(\sum_k^{c-m} c_{RM,k} - \sum_k^{c-m} c_{PM,k}\right)} \tag{35}$$

Here, x_{Ft} is the total feed composition, which is $(Fx_F + Ex_E)/(F + E)$. $\tilde{F}_t$, $\tilde{B}$ and $\tilde{R}$ are the total feed, the bottom product and the total reaction-generated flow rates in the projected space. $\tilde{\delta}_{TM}$ is the total cascade difference point for a whole column in the projected space. Note that Ξ_{NZ}, $\tilde{R}$ and $\tilde{\delta}_{TM}$ are without the stage number n in Eqs. 17, 27, and 28.

Tray-by-Tray Calculations for the Methyl Acetate Production System

Methyl acetate (MA) is produced from methanol (M) and acetic acid (AC) under a homogeneous acid catalyst. Water (W) is a byproduct in this reaction. There are two binary minimum boiling azeotropes, that is, MA-M (67 mol % of MA, 53.4°C) and MA-W (89 mol% of MA, 55.8°C), estimated from the WILSON-NTH property set in Aspen-Plus

$$CH_3COOH(AC) + CH_3OH(M) \Leftrightarrow CH_3COOCH_3(MA) + H_2O(W) \tag{36}$$

With this single reaction, we can modify the total cascade difference points in Eqs. 28 and 35 for a tray-by-tray calculation and an overall column balance in a projected composition triangle. Equations 28 and 35 are reduced into the same equation since $V_{TNZ}^T \Xi_{NZ}$ and $V_{TNZ}^T \Xi_{nNZ}$ are zero for this isomolar reaction. Here, $\bar{c}_{PMn}$ and $\bar{c}_{PM}$ are equal to $\tilde{c}_P$, and $\tilde{c}_{RMn}$ and $\tilde{c}_{RM}$ are equal to $\tilde{c}_R$. The summation of reactant coefficients (Σa_i) is 2

$$\tilde{\delta}_{TMn} = \frac{2\xi_n\left((1 - c_{P,k})\tilde{c}_P - (1 - c_{R,k})\tilde{c}_R\right)}{2\xi_n(c_{R,k} - c_{P,k})} = \frac{(1 - c_{P,k})\tilde{c}_P - (1 - c_{R,k})\tilde{c}_R}{(c_{R,k} - c_{P,k})} = \tilde{\delta}_{TM} \tag{37}$$

We perform tray-by-tray calculations only for the reactive zone between the two feedstreams, while assuming reaction equilibrium with the reaction equilibrium constant 5.2 based on the mol fractions of the mixture (Agreda et al., 1990). The equilibrium manifold is a surface in the original composition space. However, if we cut the tetrahedron into a triangle with a constant liquid composition of one of the species, the reaction equilibrium is represented by a curved line, as in Figure 7. The upper saturated liquid feed (E) contains pure AC and the lower saturated liquid feed contains pure M.

Total material balances

Table 2 shows the total cascade difference points for each projected space. In this reduced space, the reaction converts one mol of reactant (only methanol *M*, as we are ignoring AC) into products water (*W*) and methyl acetate (*MA*). For reduced set of species *M*, *W*, and *MA* in this projected space the reactant and product coefficient vectors are $[1,0,0]^T$ and $[0,1/2,1/2]^T$ ($\tilde{c}_R$ and $\tilde{c}_P$). Thus, the total cascade difference point ($\tilde{\delta}_{TM}$) in Eq. 37 is $[-1, 1, 1]^T$. Note, its terms do not sum to zero so we do not plot it at infinity. In the same way, we can obtain the total cascade difference point for other triangles as in Table 2.

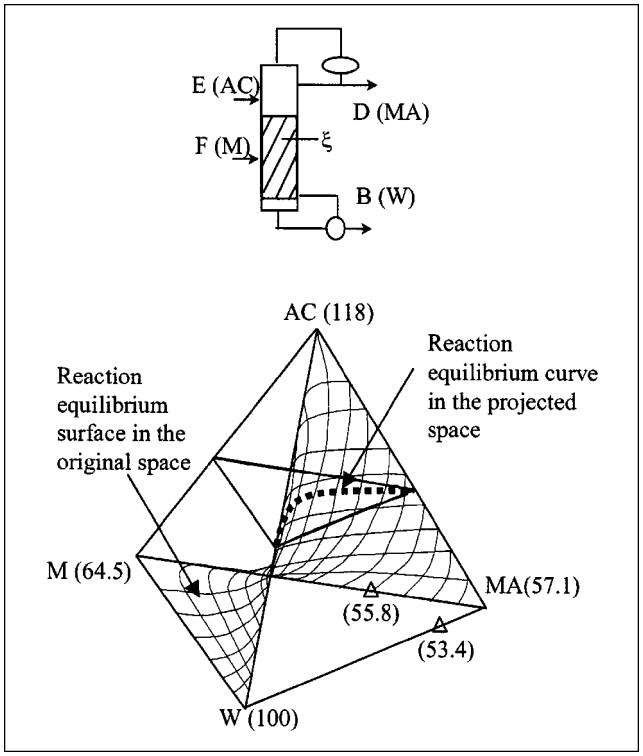

Figure 7. Methyl acetate production system at 1 atm.
Open triangles are for the binary azeotropes.

Table 2. Elements of Stoichiometric Coefficient Vectors

Constant Composition	*Vectors*	*AC*	*M*	*W*	*MA*
Original space					
	c_P	0.0	0.0	1/2	1/2
	c_R	1/2	1/2	0.0	0.0
Projected space					
AC constant ($\tilde{R}=\xi$)	$\tilde{\delta}_{TM}=\tilde{\delta}_{TMn}$		−1	1	1
	$\tilde{c}_P$		0	1/2	1/2
	$\tilde{c}_R$		1	0	0
M constant ($\tilde{R}=\xi$)	$\tilde{\delta}_{TM}=\tilde{\delta}_{TMn}$	−1		1	1
	$\tilde{c}_P$	0		1/2	1/2
	$\tilde{c}_R$	1		0	0
W constant ($\tilde{R}=-\xi$)	$\tilde{\delta}_{TM}=\tilde{\delta}_{TMn}$	1	1		−1
	$\tilde{c}_P$	0	0		1
	$\tilde{c}_R$	1/2	1/2		0
MA constant ($\tilde{R}=-\xi$)	$\tilde{\delta}_{TM}=\tilde{\delta}_{TMn}$	1	1	−1	
	$\tilde{c}_P$	0	0	1	
	$\tilde{c}_R$	1/2	1/2	0	

As in Figure 8, the projected space should satisfy the total balance (Eq. 31) around a whole column. For constant compositions of AC and M in Figures 8a and 8b respectively, Eq. 31 states that the combined point (*) lies between the total cascade difference point and the total feed composition. This combined point also lies between the top and the bottom product compositions. In the same way, the geometrical construction can be easily done for constant compositions of products MA and W.

Reaction and phase equilibrium curves in a projected space

The reaction equilibrium constant should be modified in a projected space where we hold the liquid composition of one of the species constant. For example, if the liquid composition of *AC* is constant with the value *C* (that is, $x_{AC}=C$), the reaction equilibrium constant becomes as follows

$$K_{eq}=5.2=\frac{x_{MA}x_W}{x_M x_{AC}}=\frac{x_{MA}x_W}{x_M C}=\frac{\tilde{x}_{MA}(1-C)\tilde{x}_W(1-C)}{\tilde{x}_M(1-C)C}$$

$$=\frac{(1-C)}{C}\frac{\tilde{x}_{MA}\tilde{x}_W}{\tilde{x}_M} \quad (38)$$

Since the total sum of $\tilde{x}_{MA}$, $\tilde{x}_M$ and $\tilde{x}_W$ is one in the projected space, we can draw the reaction equilibrium curve in terms of $\tilde{x}_{MA}$ and $\tilde{x}_W$, as in Figure 9. We use Eqs. 10 and 11 to construct the bubble point curve in phase equilibrium with the reaction equilibrium curve. Liquid and vapor compositions of each reactive stage are assumed to lie on the reaction equilibrium and its bubble point curves in the projected space. The liquid composition of AC $x_{n,\mathrm{AC}}$ is 0.05 in this figure and in Eq. 24. Thus, $\tilde{L}_n$ is $0.95L_n$. Since $x_{D,AC}$ is zero and $x_{E,AC}$ is one, Eqs. 25 and 26 state that $\tilde{D}$ equals D and $\tilde{E}$ zero. The reaction-generated flow rate from the top to stage n ($\tilde{R}_n$) is ξ_n in Eq. 27. Hence, Eq. 22 is rewritten as follows for tray-by-tray calculations in the projected triangle

$$\tilde{V}_{n+1}\tilde{y}_{n+1}=0.95L_n\tilde{x}_n+D\tilde{x}_D-\xi_n\tilde{\delta}_{TMn} \quad (39)$$

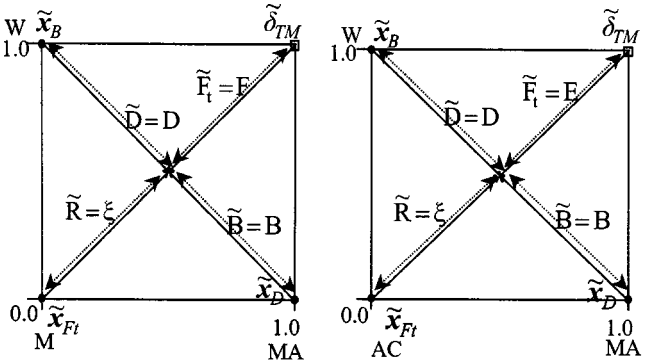

Figure 8. Reactive lever rule for total balances in the projected spaces with: (a) constant liquid composition of AC; (b) constant liquid composition of *M*.

To analyze our problem geometrically, select a reasonable by arbitrary vapor composition, $\tilde{y}_{n+1}$. We connect this given vapor composition and the total cascade difference point ($\tilde{\delta}_{TM}$) by a straight line in Figure 9. Then, according to the internal reflux ratio ($0.95L_n/D$), we locate the liquid composition ($\tilde{x}_n$) at stage n on the reaction equilibrium curve by drawing a straight line from the distillate composition, as in Figure 9. The intersection point of these two straight lines is the combined point (*) of the vapor composition and the total cascade difference point or the liquid composition and the distillate composition. The projected vapor composition ($\tilde{y}_n$) at stage n is available using the phase equilibrium relationship with $\tilde{x}_n$ in Eq. 10.

Circumventing two binary azeotropes

We can carry out one tray-by-tray calculation as noted above in the projected space with a constant liquid composition for *AC*. Our goal is to see in which direction this tray-by-tray calculation is taking us. We can include three components (*M*, *MA* and *W*) forming two binary azeotropes in this space. We can check and find that the nearby projections for

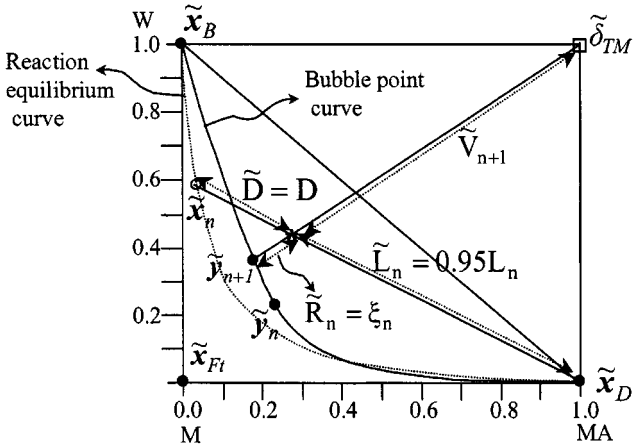

Figure 9. Tray-by-tray calculations for the given vapor composition at stage $n+1$ in the projected space when the liquid composition of acetic acid (x_{AC}) is 0.05.

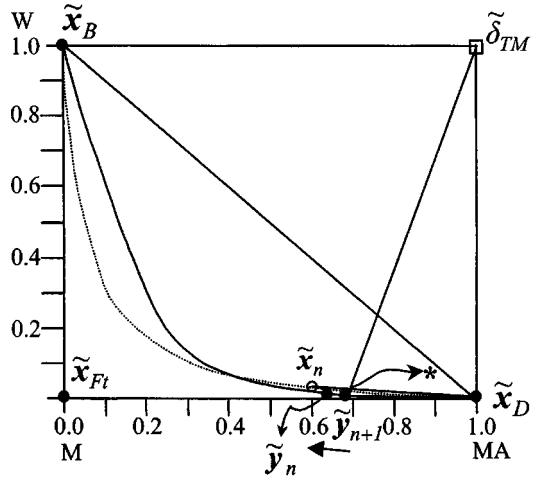

Figure 10. Tray-by-tray calculations for the given vapor composition at stage $n+1$ in the triangle with $x_{AC} = 0.05$.

The arrow shows the direction of the vapor composition vectors as we go up the column. *: combined point of $\tilde{x}_D$ and $\tilde{x}_n$ = combined point of $\tilde{\delta}_{TM}$ and $\tilde{y}_{n+1}$.

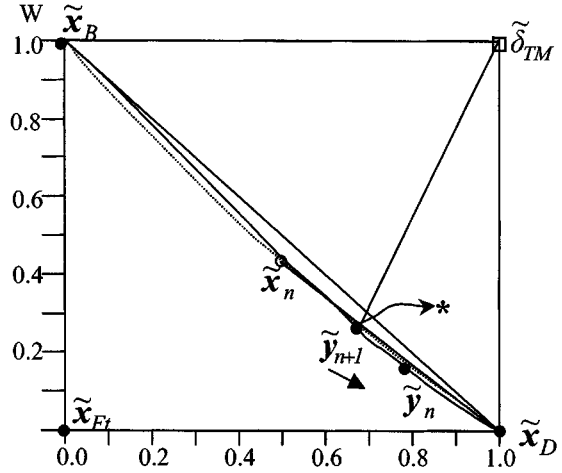

Figure 12. Tray-by-tray calculations for the given vapor composition at stage $n+1$ in the triangle with $x_{AC} = 0.4$.

The arrow shows the direction of the vapor composition vectors as we go up the column. *: combined point of $\tilde{x}_D$ and $\tilde{x}_n$ = combined point of $\tilde{\delta}_{TM}$ and $\tilde{y}_{n+1}$.

different amounts of *AC* look similar. To step up the stages within the reactive zone, we note that the composition of AC will actually increase since the *AC* is provided in the upper feedstream. We can switch from Figure 10 to Figure 11 and then to Figure 12, increasing the composition of *AC* in each. With $x_{AC} = 0.05$, the vapor composition vectors move toward the *M* vertex, (Figure 10) for the given vapor composition ($\tilde{y}_{n+1}$) and the given internal reflux ratio ($L_n/D = 3$), as we step up the stages. However, if x_{AC} is equal to and greater than 0.1 as in Figures 11 and 12, the vapor composition vectors move toward *MA* vertex, which means that, since *AC* becomes richer as we go up the column, we can circumvent the MA-M azeotrope. The reaction above stage *n* can drive the vapor composition to lie near the MA vertex. As the composition vectors approach pure MA vertex of the projected triangles which is the MA-AC binary edge in the original composition space, the nonreactive section above the reactive zone can enrich pure MA at the top from the mixture of MA and AC.

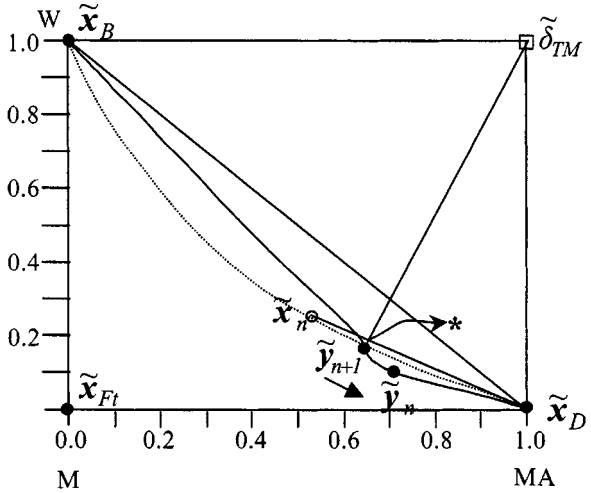

Figure 11. Tray-by-tray calculations for the given vapor composition at stage $n+1$ in the triangle with $x_{AC} = 0.1$.

The arrow shows the direction of the vapor composition vectors as we go up the column. *: combined point of $\tilde{x}_D$ and $\tilde{x}_n$ = combined point of $\tilde{\delta}_{TM}$ and $\tilde{y}_{n+1}$.

Figures 11 and 12 show that this reactive distillation column also breaks the MA-W azeotrope as we move up the column. The upper feedstream containing AC acts as an extractive agent to break the MA-W azeotrope (Agreda et al., 1990). We can already pass over this azeotrope as we move up the reaction zone just below the extraction zone. Since the reaction equilibrium curve and the bubble point curve move closer to the W-MA edge as the liquid composition of AC increases in Figures 10 to 12, the reaction conversion ($\tilde{R}_n = \xi_n$ in Figure 9) can be very small in the upper part of the reaction zone. Thus, the water content produced from the reaction is relatively small in the upper part of the reaction zone unless the reflux ratio is large. Though the extraction by AC still occurs in the extractive section above the reaction zone to remove the water, the extractive effect is not so dominant in the upper reaction zone since water is mostly produced in the lower reaction zone.

Effect of reflux ratios on reaction conversion

Assuming reaction equilibrium on reactive stages, the overall reaction conversion increases when the reflux ratio increases in the ternary reaction systems as reported in the literature (Okasinski and Doherty, 1997; Sneesby et al., 1998; Lee and Westerberg, 2000g). However, in this methyl acetate system, the overall reaction conversion can deteriorate as the reflux ratio increases.

Since the bubble point (vapor) curves in Figures 10 to 12 cross from the right side to the left side of the reaction equilibrium curve (liquid), the accumulated reaction turnover from the top to stage *n* (ξ_n) can decrease as the reflux ratio increases. For example, the reflux ratio increases when the

combined point (*) of the liquid composition ($\tilde{x}_n$) and the distillate composition ($\tilde{x}_D$) approaches the liquid composition in Figure 13. From point 4 to point 3 (the internal reflux ratio r_n increases from 1.83 to 2.84), the accumulated reaction turnover (ξ_n) slightly increases from 0.46 D to 0.47 D. But, if the combined point moves from 3 to 1 (r_n increases from 2.84 to 7.68), ξ_n is decreasing and finally becomes zero at the extreme point of 1. Here, the minimum reflux occurs at point 4 since the vapor compositions at stages n and $n+1$ are identical in this projected space.

Note, we are arguing that the projected vapor compositions being equal implies the corresponding vapor compositions in the full four component space are equal. Projecting for a constant composition for AC has a simple geometric interpretation in the full four component space. Select any composition point in full composition space and draw a line from the AC vertex through it to the triangular face opposite. The point in the opposite triangle has the projected values for the coordinates—that is, the coordinates for the other three species on an AC free basis. The bubble curve is a projection of the points we compute that are vapor equilibrium with the liquid reaction equilibrium surface. We show this surface in Figure 14. We see that equal projected points implies the same intersection point with this surface (unless the surface would exactly line up with the projection line or weave back and forth and thus intersect multiple times along the projected line). Thus, in general, equal projected bubble point compositions are the same composition in the original space. As we show the actual bubble point surface here, we see the intersections are unique here.

In this projected space, the minimum internal reflux is 1.83, which indicates that the minimum external reflux ratio ($r = L_0/D$) can be 0.83 if we exclude the upper saturated liquid feed flow rate ($E = D$) under the assumption of constant molar overflow (CMO). Agreda et al. (1990) reported the actual operating range for the external reflux ratio as 1.65 to 1.85.

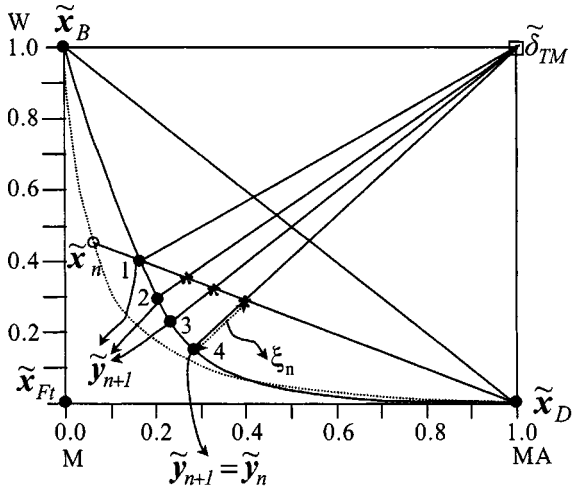

Figure 13. Relationship between reflux ratio and overall reaction conversion in the triangle.

$x_{AC} = 0.05$. 1: $r_n = 7.68$ and $\xi_n = 0.0$, 2: $r_n = 3.67$ and $\xi_n = 0.38$ D, 3:$r_n = 2.84$ and $\xi_n = 0.47$D, 4:$r_n = 1.83$ and $\xi_n = 0.46$D, *: combined point of $\tilde{x}_D$ and $\tilde{x}_n$ = combined point of $\tilde{\delta}_{TM}$ and $\tilde{y}_{n+1}$.

Also, in Figure 13, the reaction molar turnover is highest at the internal reflux of 2.84 which is 1.84 in terms of the external reflux ratio under the CMO assumption. This value for the external reflux ratio does not change much as long as we take the liquid composition ($\tilde{x}_n$) near the M-W binary edge, away from the intersection point of the reaction equilibrium and the bubble point curve in Figure 13.

Sawistowski and Pilavakis (1988) also supports this counterintuitive behavior in their simulation studies: the overall reaction conversion decreases from 60% to 50% if the external reflux increases from 4 to 30. Figure 15 shows Apsen Plus simulation results for the relationship between the external

Table 3. Simulation Results for Methyl Acetate Production System under Reaction Equilibrium

Reflux Ratio	**1**	**1.8**	**6**
Feed flow rate (kmol/h) *AC/M*	1,000/1,000	1,000/1,000	1,000/1,000
Product:			
Top flow/*MA* purity %	1,000/88.9	1,000/99.6	1,000/85.5
Bottom flow/*W* purity %	1,000/88.6	1,000/99.4	1,000/83.5
Total stages No. including condenser and reboiler	60	60	60
Feedstages:			
Upper (*AC*)/Lower (*M*)	10/50	10/50	10/50
Reactive stages	15–60	15–60	15–60
Duty (GJ/h):			
Condenser	61.75	85.27	216.6
Reboiler	29.34	50.21	185.5
Accumulated reaction turnover (kmol/h)/*AC* liquid composition at each reactive stage	$\xi_{15} = 0.39\, x_{15} = 0.79$ $\xi_{45} = 16.0\, x_{45} = 0.65$ $\xi_{49} = 295/x_{49} = 0.39$ $\xi_{50} = 736/x_{50} = 0.08$ $\xi_{60} = 893/x_{60} = 0.005$	$\xi_{15} = 0.90\, x_{15} = 0.45$ $\xi_{45} = 30.1/x_{45} = 0.44$ $\xi_{49} = 328/x_{49} = 0.39$ $\xi_{50} = 740/x_{50} = 0.10$ $\xi_{60} = 996/x_{60} = 0.004$	$\xi_{15} = 10.7/x_{15} = 0.16$ $\xi_{45} = 109/x_{45} = 0.14$ $\xi_{49} = 394/x_{49} = 0.09$ $\xi_{50} = 587/x_{50} = 0.06$ $\xi_{60} = 871/x_{60} = 0.13$
Total molar reaction conversion based on MeOH feed	89.3%	99.6%	87.1%

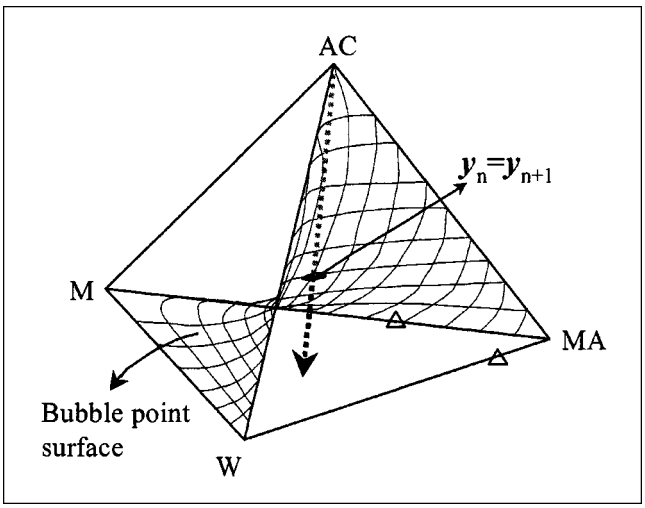

Figure 14. One intersection point of the projection line from *AC* vertex and the bubble point surface.

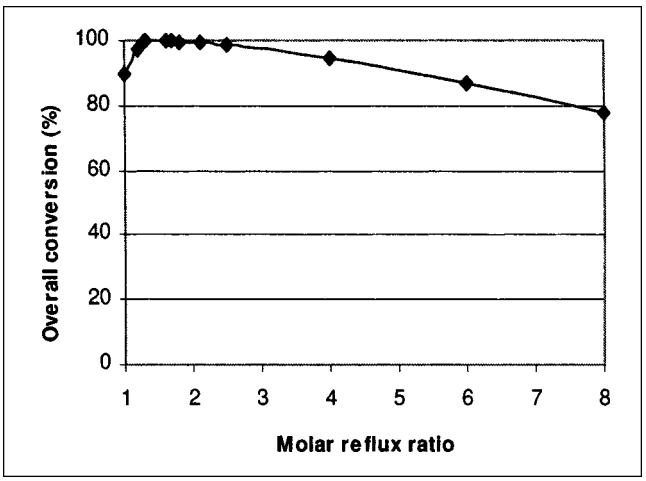

Figure 15. Relationship between the external molar reflux ratio and the overall reaction conversion.

reflux ratio and the overall reaction conversion. When the external reflux ratio is below 1.3 or above 2, the overall conversion decreases. So, the optimal range of the external reflux ratio is 1.3 to 2.0 from these simulations.

Table 3 shows the detailed simulation results for reactive distillation columns with a fixed number of stages and a fixed location of the reaction zone. The reactive section is from stages 15 to 60, and there is the extractive section from stages 10 to 14. The reaction equilibrium constant is also 5.2 based on the mol fractions, and the reflux ratio varies from 1 to 6. These simulation results shows that the overall reaction conversion decreases (99.6% to 87.1%) as the reflux ratio increases from 1.8 to 6. If the reflux ratio changes from 1.8 to 1, the reaction conversion decreases from 99.6% to 89.3%. These trends agree well with the graphical interpretation in Figure 13. As already mentioned in the previous section, Table 3 also shows that the reaction conversion in the upper part of the reaction zone is very small. For instance, the accumulated reaction turnover from reactive stages 15 to 45 (ξ_{45}) is below 12.5% of the overall reaction molar turnover in three cases of Table 3.

Here, we should clarify one point for the results in Table 3. The accumulated reaction turnover (ξ_n) decreases in Figure 13 as the reflux ratio increases, but the computer simulations in Table 3, ξ_{49} (one stage above the feedstage), increases as the reflux ratio goes from 1.8 to 6. The difference between Figure 13 and these simulations is that, while Figure 13 illustrates the effect of different reflux ratios for the same liquid composition of *AC*, these simulations in three cases show the different composition profiles under different reflux ratios.

In these simulation results, the AC liquid composition changes from stage to stage compared to the constant liquid composition of *AC* in Figure 13. It changes from 0.45 to 0.39 between stages 15 and 49 when the reflux ratio is 1.8. Thus, the reaction equilibrium curve and the bubble point curve lie very close to the W-MA binary edge, and the accumulated reaction molar turnover can be very small as in Figure 12 ($x_{AC} = 0.4$). However, as the AC liquid composition varies from 0.16 to 0.09 between stages 15 and 49 at the reflux ratio of 6, the reaction equilibrium curve and the bubble point curve can lie away from the W-MA binary edge, as in Figure 11 ($x_{AC} = 0.1$). Thus, the reaction molar turnover geometrically found in Figure 9 can be larger (ξ_n) using a reflux ratio of 6 than when using a reflux ratio of 1.8 in these simulation results. On the other hand, the overall reaction turnover (ξ_{60}) increases as the reflux ratio decreases from 6 to 1.8, which agrees to the results in Figure 13.

If the computer simulations are to exactly describe the graphical interpretation of Figure 13, the liquid composition profile at *AC* should be nearly the same when using different reflux ratios. To have nearly the same liquid composition profile of *AC* for different reflux ratios, we manipulate the top product flow rate for the same column structure in Table 3 and the given liquid composition of AC at stage 49. Table 4 shows the accumulated reaction turnovers decrease as the reflux increases from 6 to 8. The liquid composition of *AC* at stage 49 is fixed as 0.1 for all cases in Table 4. The liquid composition profiles of AC for each case are nearly the same from stages 15 to 60. For a different range of the reflux ratio, that is, from 2 to 4, the liquid composition profiles of *AC* are different from those in Table 4. In this case, we can check if the reaction molar turnovers are decreasing as the reflux increases from 2 to 4 when using nearly the same liquid composition profile of *AC*.

Conclusions

We have developed a graphical method for designing a reactive distillation column with more than three components. For the nonisomolar reaction of the methyl *tert*-butyl ether production, placing the reaction at the feed stage and in the rectifying section can circumvent the binary azeotrope between isobutene and methanol. We have derived projection equations to carry out tray-by-tray calculations using projec-

tion to reduce the dimension of the space to three, which we can more easily analyze visually. The tray-by-tray calculations for the methyl acetate production system easily show us how this reactive distillation column circumvents two minimum boiling azeotropes. This esterification reaction occurs dominantly in the lower part of the reaction zone near the lower feed stage. There is an optimal operating range for the external reflux ratio for this system. When AC liquid composition is constant as 0.05, the overall reaction conversion decreases if the current reflux ratio decreases below 0.83 or increases above 1.84. We can show how to use the proposed visualization method to perform tray-by-tray calculations for other esterification reactions. Thus, we can determine if reactive distillation will work to produce pure acetates with simple sketches.

Notation

a_{ij} = stoichiometric coefficient of reactant i and reaction j
b_{ki} = stoichiometric coefficient of product i and reaction j
B = bottom molar flow rate
$\tilde{B}$ = reduced bottom flow rate in the projected space
c = number of components
c_{Pj} = normalized product coefficient vector for reaction j
c_{PM} = normalized cascade coefficient vector of products
c_{PMn} = normalized cascade coefficient vector of products at stage n
c_{Rj} = normalized reactant coefficient vector for reaction j
c_{RM} = normalized cascade coefficient vector of reactants
c_{RMn} = normalized cascade coefficient vector of reactants at stage n
$\tilde{c}_i$ = all stoichiometric coefficient vectors in the projected space for $i = P$, PM, PMn, R, RM and RMn
$\tilde{c}_{i,k}$ = normalized reactant stoichiometric coefficient of excluded component k for $i = P$, PM, PMn, R, RM and RMn
D = distillate molar flow rate
$\tilde{D}$ = reduced distillate flow rate in the projected space
E = upper (extractive) feed molar flow rate
F_t = total feed molar flow rate
$\tilde{F}_t$ = reduced total feed flow rate
F = feed molar rate
K_{eq} = reaction equilibrium constant
K_i = phase equilibrium constant for species i
K'_i = phase equilibrium constant for species i in the projected space
L_n = liquid molar flow rate at stage n
$\tilde{L}_n$ = reduced liquid flow rate at stage n
l = index for key components in the projected space, $l = 1, \ldots, m$
m = number of key components in the projected space
Np = number of products
Nr = number of reactants
NR = number of reactions
NZ = number of nonzero cases for the total sum of stoichiometric coefficients
r = external reflux ratio (L_0/D)
r_n = internal reflux ratio (L_n/D)
R_i = reactant i
P_k = product k
$\tilde{R}$ = reduced reaction-generated flow rate in a whole column
$\tilde{R}_n$ = reduced reaction-generated flow rate at stage n
V_n = vapor molar flow rate at stage n
$\tilde{V}_n$ = reduced vapor flow rate at stage n
x_{Fs}, y_{Fs} = liquid and vapor composition at the feed stage
x_i = vapor composition for component i
$x_{i,k}$ = liquid composition with excluded component k for stream $i = B$, D, E, F_t, and stage n
x_i = liquid composition vector for stream $i = B$, D, E, F, F_t
$\tilde{x}_i$ = all liquid composition vector in the projected space for stream $i = B$, D, E, F, F_t and stage n
$\tilde{x}_l$ = liquid composition in the projected space for component l
y_i = vapor composition for component i
$y_{i,k}$ = vapor component with excluded component k for stream $i = B$, D, E, F_t and stage n
y_n = vapor composition vector at stage n
$\tilde{y}_i$ = all vapor composition vector in the projected space for stage i
$\tilde{y}_l$ = vapor composition in the projected space for component l
Z = number of zero cases in the total sum of stoichiometric coefficients

Greek letters

δ_{Rl} = reaction difference point of reaction l
δ_{RM} = cascade reaction difference point
δ_{RMn} = cascade reaction difference point at the stage n
δ_{TM} = total cascade difference point
δ_{TMn} = total cascade point at the stage n
$\delta_{i,k}$ = reaction difference composition with excluded component k

Table 4. Accumulated Reaction Molar Turnovers for Different Reflux Ratios

Reflux Ratio	**6**	**7**	**8**
Feed flow rate (kmol/h) *AC/M*	1,000/1,000	1,000/1,000	1,000/1,000
Product:			
Top flow/*MA* purity %	987.1/85.8	856.6/84.6	756.0/83.3
Bottom flow/*W* purity %	1,012.9/82.3	1,143.4/68.9	1,244.0/61.1
Total stages No. including condenser and reboiler	60	60	60
Feedstages:			
Upper (*AC*)/Lower (*M*)	10/50	10/50	10/50
Reactive stages	15–60	15–60	15–60
Accumulated reaction turnover (kmol/h)/*AC* liquid composition at each reactive stage	$\xi_{15} = 10.5/x_{15} = 0.161$ $\xi_{30} = 38.2/x_{30} = 0.156$ $\xi_{45} = 108/x_{45} = 0.145$ $\xi_{49} = 393/x_{49} = 0.100$ $\xi_{50} = 589/x_{50} = 0.061$ $\xi_{60} = 869/x_{60} = 0.130$	$\xi_{15} = 10.2/x_{15} = 0.158$ $\xi_{30} = 36.9/x_{30} = 0.154$ $\xi_{45} = 104/x_{45} = 0.143$ $\xi_{49} = 383/x_{49} = 0.100$ $\xi_{50} = 580/x_{50} = 0.062$ $\xi_{60} = 819/x_{60} = 0.158$	$\xi_{15} = 9.93/x_{15} = 0.157$ $\xi_{30} = 35.9/x_{30} = 0.153$ $\xi_{45} = 101/x_{45} = 0.142$ $\xi_{49} = 376/x_{49} = 0.100$ $\xi_{50} = 574/x_{50} = 0.062$ $\xi_{60} = 791/x_{60} = 0.168$
Total molar reaction conversion based on MeOH feed	86.9%	81.9%	79.1%

for $i = P$, PM, PMn, RM, RMn, TM and TMn

$\tilde{\delta}_i$ = reaction difference point in the projected space $i = P$, PM, PMn, R, RMn, TM and TMn

V = matrix consisting of stoichiometric coefficients for all reactions

V_T = row vector consisting of the elements from the sum of the total stoichiometric coefficients

V_{TNZ} = row vector consisting of nonzero elements of the sum of the total stoichiometric coefficients ($\sum b_k - \sum a_i$ = nonzero in Eqs. 16–18)

Ξ = column vector of the sum of the total molar turnover for NR different reations.

Ξ_{NZ} = column vector consisting of nonzero elements of Ξ

Ξ_n = column vector of the cumulative sum of the molar turnovers for NR reactions

ξ_{nj} = sum of the total molar turnover for j reaction from the top to n stages

ξ = total molar turnover of a reaction per unit time in a column for a single reaction

$\Delta\xi_n$ = net reaction molar turnover flow rate at stage n ($\xi_n - \xi_{n-1}$)

Literature Cited

Agreda, V. H., and L. R. Partin, ''Reactive Distillation Process for The Production of Methyl Acetate,'' U.S. Patent No. 4,435,595 (1984).

Agreda, V. H., L. R. Partin, and W. H. Heise, ''High Purity Methyl Acetate via Reactive Distillation,'' *Chem. Eng. Prog.*, **86**(2), 40 (Feb. 1990).

Al-Jarallah, A. M., M. A. B. Siddiqui, and A. K. K. Lee, ''Kinetics of Methyl Tertiary Butyl Ether Synthesis Catalyzed by Sulfuric Acid,'' *Chem. Eng. J.*, **39**, 169 (1988).

Lee, J. W., S. Hauan, K. M. Lien, and A. W. Westerberg, ''Difference Points in Extractive and Reactive Cascade II-Generating Design Alternatives by Lever Rule for Reactive Systems,'' *Chem. Eng. Sci.*, **55**, 3161 (2000a).

Lee, J. W., S. Hauan, K. M. Lien, and A. W. Westerberg, ''A Graphical Method for Designing Reactive Distillation Columns I-The Ponchon-Savarit Diagram,'' *Proc. R. Soc. Lond.*, **456**, 1953 (2000b).

Lee, J. W., S. Hauan, K. M. Lien, and A. W. Westerberg, ''A Graphical Method for Desgining Reactive Distillation Columns II-The McCabe-Thiele Diagram,'' *Proc. R. Soc. Lond.*, **456**, 1965 (2000c).

Lee, J. W., S. Hauan, and A. W. Westerberg, ''Circumventing an Azeotrope in Reactive Distillation,'' *Ind. Eng. Chem. Res.*, **39**, 1061 (2000d).

Lee, J. W., S. Hauan, and A. W. Westerberg, ''Graphical Methods for Reaction Distribution in a Reactive Distillation Column,'' *AIChE J.*, **46**, 1218 (2000e).

Lee, J. W., S. Hauan, and A. W. Westerberg, ''Extreme Conditions in Binary Reactive Distillation,'' *AIChE J.*, **46**, 2225 (2000f).

Lee, J. W., and A. W. Westerberg, ''Visualization of Stage Calculations in Ternary Reacting Mixtures,'' *Comp. Chem. Eng.*, **24**, 639 (2000g).

Nocca, J.-L., J. Leonard, J.-F. Gaillard, and P. Amigues, ''Process for The Manufacturing a Tertiary Alkyl Ether by Reactive Distillation,'' U.S. Patent No. 4,847,431 (1989).

Okasinski, M. J., and M. F. Doherty, ''Effects of Unfavorable Thermodynamics on Reactive Distillation Column Design,'' *Inst. Chem. Eng. Symp. Ser.*, **2**, 695 (1997).

Okasinski, M. J. and M. F. Doherty, ''Design Method for Kinetically Controlled, Staged Reactive Distillation Columns,'' *Ind. Eng. Chem. Res.*, **37**, 2821 (1998).

Preston, K. L., ''Use of Reactive Distillation in The Manufacture of Methyl Tert Butyl Ether,'' U.S. Patent No. 5,741,953 (1998).

Rehfinger, A., and U. Hoffmann, ''Kinetics of Methyl Tertiary Butyl Ether Liquid Phase Synthesis Catalyzed by Ion Exchange Resin-I. Intrinsic Rate Expression in Liquid Phase Activities,'' *Chem. Eng. Sci.*, **45**, 1605 (1990).

Smith, L. A., ''Catalytic Distillation Process,'' U.S. Patent No. 4,307,254, (1981).

Smith, L. A., ''Process for The Preparation of MTBE,'' U.S. Patent No. 5,118,873, (1992).

Sneesby, M. G., M. O. Tadé, R. Datta and T. N. Smith, ''Detrimental Influence of Excessive Fractionation on Reactive Distillation,'' *AIChE J.*, **44**, 388 (1998).

Sawistowski, H., and P. A. Pilavakis, ''Performance of Esterification in a Reaction-Distillation Column,'' *Chem. Eng. Sci.*, **43**, 355 (1988).

Venimadhavan, G., G. Buzad, M. F. Doherty, ''Effects of Kinetics on Residue Curve Maps for Reactive Distillation,'' *AIChE J.*, **40**, 1814 (1994).

Manuscript received May 16, 2000, and revision received Dec. 15, 2000.